High Resolution Viscosity Measurement by Thermal Noise Detection

Felipe A. Aguilar Sandoval, Manuel Sepúlveda, Ludovic Bellon, Francisco Melo

Sensors **2015**, *15*, 27905-27916; doi:10.3390/s151127905

OPEN ACCESS
sensors
ISSN 1424-8220
www.mdpi.com/journal/sensors

Article

High Resolution Viscosity Measurement by Thermal Noise Detection

Felipe Aguilar Sandoval [1,†,*], Manuel Sepúlveda [1,†], Ludovic Bellon [2,†] and Francisco Melo [1,†,*]

[1] Departamento de Física, Universidad de Santiago de Chile, Avenida Ecuador 3493, Estación Central, Santiago 9170124, Chile; E-Mail: manuel.sepulveda@usach.cl

[2] Laboratoire de Physique, Université de Lyon, Ecole Normale Supérieure de Lyon, CNRS, 46 Allée d'Italie, Lyon F-69007, France; E-Mail: ludovic.bellon@ens-lyon.fr

† These authors contributed equally to this work.

* Authors to whom correspondence should be addressed; E-Mails: felipe.aguilarsan@usach.cl (F.A.S.); francisco.melo@usach.cl (F.M.); Tel.: +56-2-2718-1209.

Academic Editor: Vittorio M. N. Passaro

Received: 21 September 2015 / Accepted: 29 October 2015 / Published: 3 November 2015

Abstract: An interferometric method is implemented in order to accurately assess the thermal fluctuations of a micro-cantilever sensor in liquid environments. The power spectrum density (PSD) of thermal fluctuations together with Sader's model of the cantilever allow for the indirect measurement of the liquid viscosity with good accuracy. The good quality of the deflection signal and the characteristic low noise of the instrument allow for the detection and corrections of drawbacks due to both the cantilever shape irregularities and the uncertainties on the position of the laser spot at the fluctuating end of the cantilever. Variation of viscosity below $0.03\,\mathrm{mPa{\cdot}s}$ was detected with the alternative to achieve measurements with a volume as low as $50\,\mu\mathrm{L}$.

Keywords: thermal fluctuations; viscosity in liquids; MEMS

1. Introduction

The measurement of rheological properties, like fluid viscosity, is of common interest in several science fields, ranging from engineering to biology, with applications including process control [1–4] and fluids' analysis for diseases diagnosis [5–7]. On the other hand, atomic force microscopy (AFM)

has became a valuable technique that is applied transversely to scientific disciplines. AFM can be used in diverse modes to image either hard or soft surfaces in both dry and fluid environment [8,9]. Besides atomic resolution imaging, force spectroscopy has emerged as a powerful tool to characterize the mechanics of soft materials at the nanoscale [10–12] and single molecule level [13].

Moreover, a new class of miniaturized, highly sensitive biosensors has been envisioned based on the high sensitivity of micro-fabricated silicon cantilevers to bending [14,15]. The selective adsorption of molecules onto the cantilever surface induces surface stresses, which ultimately leads to a deflection signal. Thermal noise detection is a less known and promising technique that has proven useful for the characterization of the cantilever mechanics [16] and its surrounding media [17,18].

In order to explore the advantages of cantilevers as sensors for fluid properties in applications in which only a small amount of material is available and where a good time response is required, we developed a device able to measure thermal fluctuations of a cantilever in the testing fluid environment, with high accuracy. We extended the capabilities of a previously-developed interferometric AFM working in gases [19] to liquid environments and recently tested in biological single-molecule experiments [20]. The analysis of the power spectrum density (PSD) of the fluctuating cantilever-deflection, through Sader's model [21], allows for the measurement of the fluid viscosity.

Previous works have used Sader's model and the optical lever method [10] for detecting deflections and deducing fluid viscosity [22–26]. In general, the information obtained was through a partial fit of the PSD spectra (p.e.of the first resonance) [24] or by solving an approximated equation system to link the frequency shift and the quality factor to the fluid viscosity and density [25], which ultimately led to accuracy of about 5%. In this article, we present the advantage of an interferometric method [19] to achieve improved PSD measurements, in order to obtain a reliable fit of the whole spectrum with Sader's model for the two first normal modes of the cantilever immersed in a liquid, which adds a quality test to the fit. This procedure simultaneously allows us for the absolute measurement of the viscosity. In addition, the micro-cantilever is actuated only by thermal noise, reducing the equipment needed to implement our method, in comparison with an externally-excited cantilever methodology (this work uses only thermal noise instead of an external cantilever excitation; however, high performance external devices [27–29] for cantilever excitation combined with our interferometer are an interesting avenue to explore in order to reduce or compensate temperature influence and other undesirable effects). Our sensing configuration requires a small amount of fluid, ranging from $1\,\mathrm{mL}$, for full immersion of the cantilever holder, to a drop of $50\,\mu\mathrm{L}$, which is the minimum amount filling the gap between the cantilever and the optical window. This last option is well suited for expensive and scarce fluids and biological samples [25].

The article is structured as follows. In Section 2, we describe the model used to fit our experimental data. Section 3 presents the improvement of the interferometer described in [19] to extend its application in liquid media. In Section 4, we describe the methodology and the protocols to prepare testing fluids and to perform measurements. Section 5 presents the obtained values of viscosity and comparisons with reference values. Finally, Section 6 discusses the results' validity, compares the model with the experimental PSD and considers the effect of the microcantilever geometry, previous to the general conclusions of this work.

2. Theory

According to Sader's theory [21] and Bellon's article [30], the PSD for each normal mode of the deflection d for a microcantilever immersed into a thermal bath at temperature T is:

$$S_{d_n}(\omega) = \frac{2k_BT}{\pi} \frac{\gamma_{\text{eff}}(\omega)}{(k_n - m_{\text{eff}}(\omega)\omega)^2 + (\gamma_{\text{eff}}(\omega)\omega^2)^2} \tag{1}$$

where d_n is the amplitude of the $n-$-th normal mode of the cantilever and a fluctuating variable due to the thermal bath, $\gamma_{\text{eff}}(\omega)$ is the frequency-dependent effective damping coefficient, $m_{\text{eff}}(\omega)$ is the frequency-dependent effective mass, k_n is the stiffness of the $n-$-th mode, k_B is the Boltzmann constant and ω is the angular frequency. The effective values m_{eff} and γ_{eff} are:

$$m_{\text{eff}}(\omega) = m + m_f\Gamma_r(\omega) \tag{2}$$

$$\gamma_{\text{eff}}(\omega) = m_f\omega\Gamma_i(\omega) \tag{3}$$

where m is the mass of the cantilever, $m_{\text{f}} = \pi\rho LW^2/4$ is the mass of the cylinder of a fluid of density ρ surrounding the cantilever of length L and width W and $\Gamma = \Gamma_r + i\Gamma_i$ is the hydrodynamic function in Sader's model context, whose values are dependent on the fluid density and viscosity. For the sake of completeness, we introduce explicitly the hydrodynamic function for a rectangular beam:

$$\Gamma(\omega) = \Omega(\omega)\Gamma_{\text{circ}}(\omega) \tag{4}$$

where Γ_{circ} is the hydrodynamic function for a cylinder expressed as:

$$\Gamma_{\text{circ}}(\omega) = 1 + \frac{4iK_1(-i\sqrt{i\text{Re}})}{\sqrt{i\text{Re}}K_0(-i\sqrt{i\text{Re}})} \tag{5}$$

where K_0 and K_1 are modified Bessel functions of the third kind and Re is the Reynolds number, expressed as:

$$\text{Re} = \frac{\rho W^2\omega}{4\eta} \tag{6}$$

where ρ is the density of the fluid where the cantilever is immersed, W is the width of the cantilever and η is the viscosity of the fluid. $\Omega(\omega)$ is a correction function, expressed in the real and imaginary parts as:

$$\begin{aligned}
\Omega_r(\omega) &= (0.91324 - 0.48274r + 0.46842r^2 - 0.12886r^3 \\
&+ 0.044055r^4 - 0.0035117r^5 + 0.00069085r^6) \\
&\times (1 - 0.56964r + 0.48690r^2 - 0.13444r^3 \\
&+ 0.045155r^4 - 0.0035862r^5 \\
&+ 0.00069085r^6)^{-1} \qquad (7) \\
\Omega_i(\omega) &= (-0.024134 - 0.029256r + 0.016294r^2 \\
&- 0.00010961r^3 + 0.000064577r^4 \\
&- 0.000044510r^5) \times (1 - 0.59702r + 0.55182r^2 \\
&- 0.18357r^3 + 0.079156r^4 - 0.014369r^5 \\
&+ 0.0028361r^6)^{-1} \qquad (8) \\
r &= \log_{10}(\text{Re}) \qquad (9)
\end{aligned}$$

where $\Omega(\omega) = \Omega_r + i\Omega_i$. The physical origin of the hydrodynamic function can be found in Sader's work [21]. It is worth nothing that in Sader's model, the dissipation is assumed homogeneous along the cantilever. If in addition, the thermal noise is uncorrelated on different normal modes [30], the PSD of the deflection d is written as:

$$S_d(x,\omega) = \sum_{n=1}^{\infty} S_{d_n}(\omega)\,|\phi_n(x)|^2 \tag{10}$$

where ϕ_n are the basis of normal modes and x is the spatial coordinate along the cantilever length (the position where the deflection is measured).

As an illustrative example, we plot the PSD of the deflection of the cantilever (Figure 1) using Equation (1) and the geometric parameters of the cantilever described in the experimental section. The PSD is computed for different values of viscosities and densities obtained for water solutions of different concentrations of glycerol that are listed in Table 1 at 24 °C and computed through the work of Cheng *et al.* [31]. A frequency shift of the resonance peaks together with significant broadening and amplitude variation are clearly observed, illustrating the sensitivity of the PSD to viscosity variations.

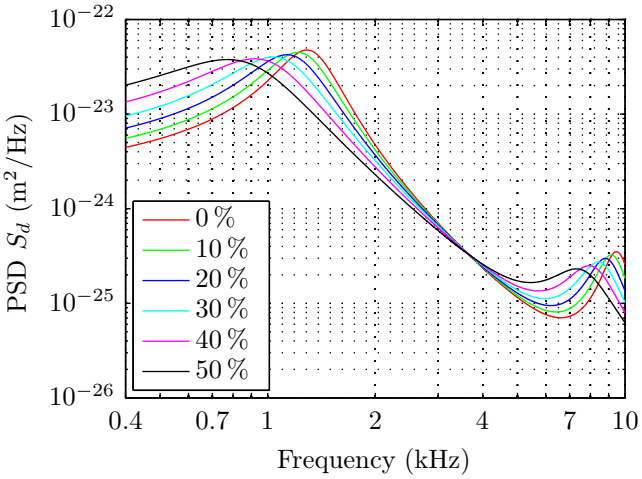

Figure 1. Theoretical curves of PSD of thermal noise-induced deflection of a cantilever for Sader's model for different glycerol concentrations, at 24 °C ; the corresponding viscosities and densities are listed in Table 1. Effects on the PSD amplitude, width and resonant frequencies are clearly visible. The geometry of the cantilever for this modeling is a length $L = 350\,\mu\text{m}$, a width $W = 32.5\,\mu\text{m}$ and a thickness $H = 1.0\,\mu\text{m}$.

Table 1. Reference values [31] of viscosity η_{ref} and density ρ_{ref} are listed for different volume concentrations of glycerol $[G]_v$ used at a temperature of 24 °C.

$[G]_v$ (%v/v)	η_{ref} (mPa·s)	ρ_{ref} kg/m^3
0	0.9135	997.1
10	1.2501	1029.7
20	1.7784	1060.6
30	2.6529	1090.0
40	4.1971	1118.0
50	7.1505	1144.7

3. Setup

3.1. Sensing

Our device is an interferometric AFM, originally designed for nano-mechanical measurements of thermal noise in a gaseous environment. The working principle and a detailed description of the interferometer can be found in [19]. The principle applied for sensing deflection is of the interferometric kind; a stable reference beam is located outside of the fluid cell using a Michelson-like polarized setup. An external mirror (M) reflects the reference beam and provides fine control of the overlap of the returned beams. A lens (L) whose fine position is controlled through a motorized three-axis system focuses the probe beam (z-control) and allows one to position the resulting laser spot at the free end of the cantilever (C) with good accuracy. This configuration allows for fine tuning, maximizing the contrast signal significantly (Figure 2). This also helps to minimize the undesirable effects of the refraction at the interfaces due to small misalignment of the probe beam. The higher resolution reached with the interferometric detection is due to the null dependence of the sensitivity with respect to the phase difference between the reference and probe beam. Thus, the background noise is limited just by the shot noise of the photodiodes. The other advantage is the deflection detection range, which can reach several microns with suitable functions in the data acquisition system. This feature is due to an automatized system detecting the unwrapped phase.

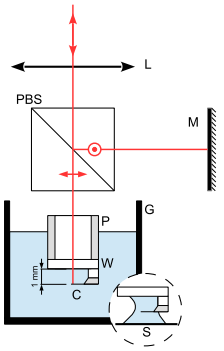

Figure 2. Using a polarized beam splitter (PBS), the input beam is divided in two, with crossed polarizations as shown in the divided laser beam. An external mirror (M) reflects the reference beam and provides fine control of the overlap of the returned beams. A lens (L) focuses the probe beam at the free end of the cantilever (C). The reflected beams, probe and reference are superposed after the PBS. Interferences are obtained after projecting the initial polarizations in the analysis area (see [19] for details). The sensing beam path is protected by a stainless steel pipe (P). An optical quality window (W) ensures the transition from air to liquid with minimum refraction and undesirable reflections in order to reach the free end of the cantilever (C). The liquid is contained in a Pyrex glass (G). Inset: the micro-droplet configuration uses a microscope slide to support a liquid drop (50 µL). The micro-cantilever is fully immersed, and the space between the window (W) and the microscope slide (S) is filled with the fluid, forming a meniscus. In order to prevent beam distortion, the window W is of laser quality with suitable anti-reflection coating.

3.2. Immersion Area and Fluid Cell

The cantilever holder for immersion in liquids is a small stainless steel pipe closed at one end by a laser quality coated window that is glued with optical UV adhesive (NOA 81, Norland Products Inc., Cranbury, NJ, USA) (Figure 2). This configuration provides a suitable transition from air to liquid, avoiding drawbacks due to refraction and undesirable reflections. The whole interferometer (including the components of Figure 2) is mounted on a manual translation microscope turret, which provides vertical motion and allows introduction of the micro-cantilever into the liquid gently. The interferometer is then moved downward until the fluid has filled the gap between the cantilever and the optical window. An alternative configuration is obtained by replacing the glass cell G (Figure 2) with a microscope slide to locate a drop ($\sim$50 µL) of fluid sample just below the cantilever (see the inset of Figure 2). This option is recommended for scarce liquids and biological fluids available only in small quantities.

4. Methods

The cantilever used for our experiments has a rectangular geometry, with nominal values of $L = 350\,\mu\mathrm{m}$ in length, $W = 33.5\,\mu\mathrm{m}$ in width and $H = 1.0\,\mu\mathrm{m}$ in thickness (MikroMasch, HQ:CSC38/Cr-Au). Notice that the nominal width is the average across the thickness, because the cantilever cross-section is trapezoidal. For a fine tuning of the mechanical properties and geometry of the cantilever, we consider as an input and as absolute values of viscosity and density those of mQ water. Indeed, with this fixed value of viscosity and fluid density, through small adjustments of the cantilever geometry, length, width and thickness, in the model, we reproduce the PSD obtained experimentally with pure water. This procedure allows one to find effective values featuring the cantilever geometry by correcting uncertainties due to irregularities of the geometrical form of the cantilever. In addition, it is important to mention that the position of the cantilever with respect to the spot of the sensing laser can be determined by scanning the cantilever with the same laser spot, using a micro-positioning system. Thus, the laser spot can be positioned at the desired position x near the free end of the cantilever ($x = L$). Notice that knowing the exact point on the cantilever at which thermal fluctuations are detected is crucial for a good repeatability and accuracy in the fit procedure, because the theoretical PSD is calculated for this particular point at the cantilever. We realized that fine tuning of this parameter improved the fit quality; therefore, it was allowed to slightly vary in the fitting procedure.

As reference fluids, we use different volume concentrations of glycerol, from $1\,\%$ to $50\,\%$. The density ρ_{ref} and the viscosity η_{ref} values used as reference data were computed using an empirical equation [31]. The volume of each reference fluid used in the experimental cell was $1\,\mathrm{mL}$. When performing the measurements, the temperature variation from run to run was corrected. To prevent rapid temperature variations, the whole setup was enclosed in an acrylic box, and the fluid was allowed to thermalize prior to measurements. Two thermometers in the acrylic box allowed for the temperature monitoring. A digital thermometer with a resolution of 0.1 °C registered temperature in the enclosure, whereas a thermocouple located in contact with the glass window (W) monitored the sample temperature. We whole variation of temperature during the experiments was kept smaller than 0.1 °C.

Two sets of reference fluids were prepared with two different protocols. The first group of fluids ranges from $1\,\%$ to $10\,\%$ of glycerol and is obtained from a seed dilution of $10\,\%$ glycerol by gradual

dilution in steps of 1 %. The second group includes concentrations from 10 % to 50 % in steps of 10 %, and these were prepared one by one. All mixtures were prepared with mQ water.

5. Results

The measurements were divided by concentration in two groups of testing fluids; one from 0% to 9% glycerol in steps of 1% and the other from 10% to 50% glycerol in steps of 10%. The experimental PSD of the deflection for different concentrations (Figure 3) shows that the effect of viscosity variations produces both a noticeable frequency shift and a resonance widening for increasing glycerol concentration. The quality of the fitting for the whole PSD is shown in Figure 4.

For the first group (concentrations from pure water to 9 % of glycerol), the viscosities η_{exp} obtained by fitting the PSD are compared to the reference values η_{ref} in Table 2. Errors up to 1 % are obtained, although in most cases, the errors are much smaller, with a mean value of 0.5 % for this first group of measurements. We conclude that our procedure allows for the detection of viscosity variations as low as 1 %, differentiating changes below 0.03 mPa·s. Values of the cantilever's geometry obtained from the fitting procedure, width W_f and length L_f are $L_f = 354$ µm, $W_f = 32.9$ µm, which compare well to the nominal values, $L = 359$ µm and $W = 33.5$ µm.

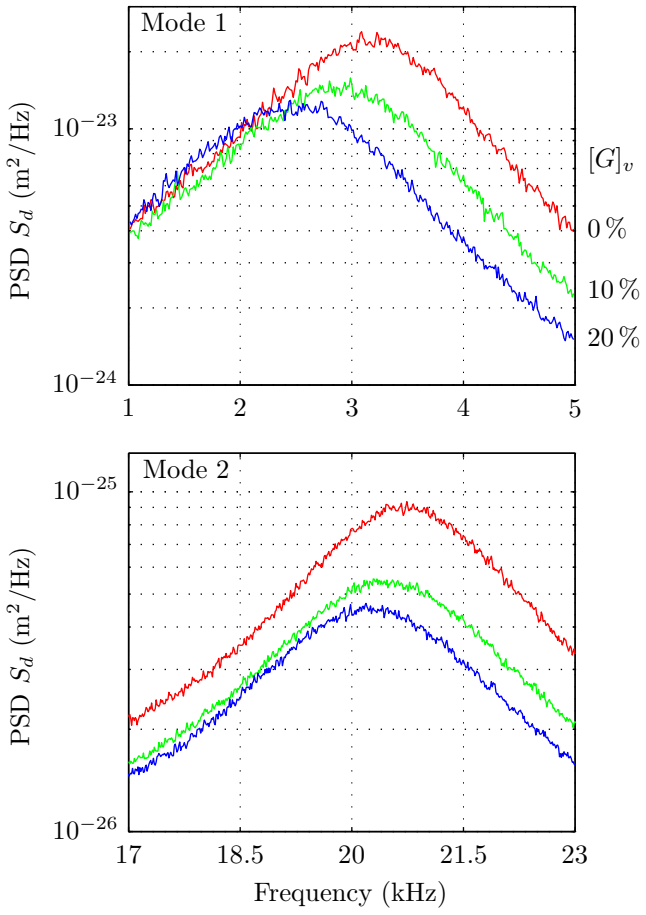

Figure 3. Zoom around the two first resonances of the thermal noise spectra of the deflection of a cantilever immersed in water-glycerol mixtures. These PSDs show increasing frequency shifts and resonances widening for increasing glycerol concentration.

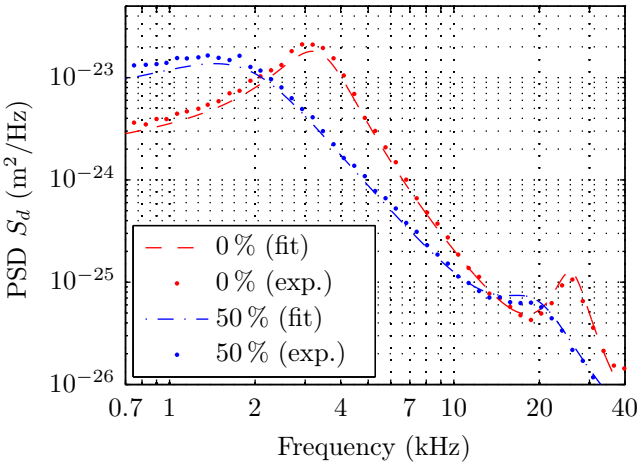

Figure 4. Experimental data (dots) and fits with Sader's model (dashed lines) for the PSD of thermal noise-induced deflection for pure water (mQ) and a solution of 50% of glycerol.

Table 2. Comparison between reference viscosities η_{ref} and those extracted from the fits of the PSDs of the measured thermal noise η_{exp}, for mixtures of water and glycerol in the range of zero to 10 %.

$[G]_v$ (%v/v)	η_{ref} (mPa·s)	η_{exp} (mPa·s)	error (%)
0	0.913	0.912	−0.07
1	0.938	0.940	0.16
2	0.967	0.957	−1.11
3	0.995	0.993	−0.23
4	1.026	1.029	0.30
5	1.058	1.062	0.38
6	1.092	1.096	0.35
7	1.125	1.125	0.04
8	1.162	1.177	1.34
9	1.200	1.212	0.98

In turn, for concentrations from 10 % to 50 % of glycerol, the measured viscosity has bigger errors with respect to the reference value, as seen in Table 3. Such increasing errors are expected and demonstrate that our procedure for tuning cantilever parameters (performed with pure water) is valid for about one order of magnitude variation in viscosity with a maximum error less than 10 %.

Table 3. Comparison between reference viscosities η_{ref} and those extracted from the fits of the PSDs of the measured thermal noise η_{exp}, for mixtures of water and glycerol in the range of 10 % to 50 %.

$[G]_v$ (%v/v)	η_{ref} (mPa·s)	η_{exp}(mPa·s)	error (%)
10	1.256	1.278	1.7
20	1.783	1.785	0.1
30	2.661	2.580	–3.0
40	4.197	4.047	–3.6
50	7.150	6.573	–8.1

6. Discussions

In additional experiments, we tested the performance of a different cantilever, the Arrow TL1 (NanoWorld, without coating), of nominal values $L = 500\,\mu\text{m}$, $W = 100\,\mu\text{m}$ and $1\,\mu\text{m}$ thickness. The viscosity values obtained with this cantilever (not presented here), under the same conditions, differ from those obtained with MikroMasch. First, we observed that when the nominal values of W and L are used, viscosities values resulted in being unrealistic, revealing an inaccuracy. Second, when W and L are used as free parameters to adjust the PSD of pure water with the value of pure water viscosity as an input, the equivalent L and W ($471\,\mu\text{m}$ and $77\,\mu\text{m}$, respectively) differed from nominal values, confirming the previous inaccuracy. With these parameters, the measured values of viscosities differed about 4% with respect to the reference ones (for the set 1% to 10% glycerol). In addition, we detected a mismatch between two adjacent modes with respect to the model used (Figure 5a). It was not possible to fit both resonances with a single set of parameters, which further questions the trust of the fit. Our experiments suggest that these effects are due to the size of the triangular head (about $85\,\mu\text{m}$) of the Arrow TL1 relative to its total length. Indeed, the MikroMasch cantilever also has a triangular end; however, its size is only about $20\,\mu\text{m}$, which is small compared to the cantilever total length. Figure 6 show pictures for the comparison of the free ends of both cantilevers. We concluded that the effect of the shape of the cantilever end is reduced by considering large aspect ratio cantilevers. In the case of the MikroMasch cantilever, a fine tuning of W and L allows for reducing errors in viscosity from 3% to 1%.

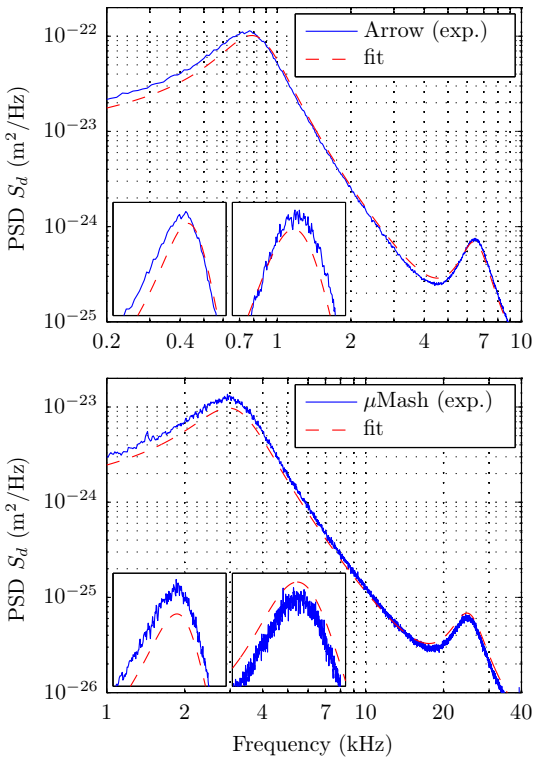

Figure 5. Comparisons of the quality of the fits of the PSDs for both cantilevers used. (**Top**) The Arrow TL1, NanoWorld cantilever produces an optimized fit that has a notorious mismatch in the resonances frequencies. Insets: details of the fits for the first and the second cantilever resonance; (**Bottom**) Same as the top curve for the MikroMasch (HQ:CSC38) cantilever. Insets: the fit with the Sader's model captures both resonances simultaneously.

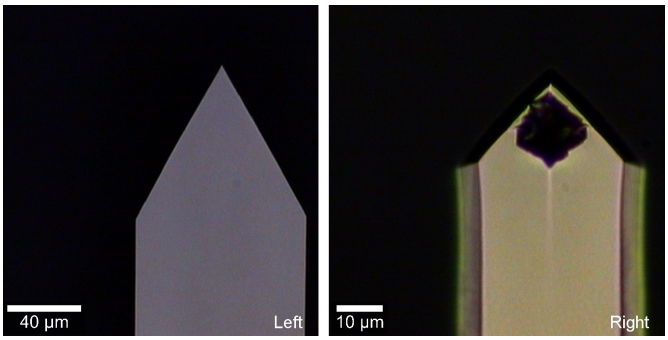

Figure 6. Calibrated images of the end of the cantilevers. (**Left**) Arrow TL1 cantilever; (**Right**) MikroMasch cantilever.

In spite of these subtle geometrical effects, which could offer opportunities for further improvements in the use of micro-cantilevers for viscosity measurements, our methodology allows for the detection of viscosity changes as low as 1%. The errors relative to the reference values increase when the changes of viscosity are greater than $30\,\%$.

7. Conclusions

The interferometric detection for cantilever deflection enables the measurement of the PSD of thermal fluctuations with a very high resolution and low noise. This is useful to discriminate small changes of the viscosity of the surrounding media of the cantilever in less than $0.03\,\mathrm{mPa{\cdot}s}$. The amount of liquid needed to perform the measurements is an additional advantage of the method, allowing volumes as small as $50\,\mu\mathrm{L}$. Regarding the time resolution of the method, measurements as fast as four data points per minute have been achieved, which suggests that the methodology is well adapted to follow the time evolution of fluid viscosity, due to either structural changes in complex fluids or variations of some external parameter. However, the fluid under scope must be sufficiently transparent and free of impurities, producing scattering and perturbation of the probe beam.

The geometry of the micro-cantilever used was shown to play an important role: we observed that the triangular end of the cantilever can modify significantly its equivalent dimensions and the relation between their resonance frequencies, as the model no longer accurately captures the resonance frequencies simultaneously. Thus, our results suggest that further improvements in fluid property measurements can be made through the optimization of the cantilevers' geometry.

Acknowledgments

We thank G. Martin for technical assistance and A. Petrosyan for valuable suggestions. This work has been supported by Fondecyt, Chile, under Grant No. 1130922 and Proyecto DICYT041331 MHPOSTDOC.

Author Contributions

F. Melo, F. Aguilar and L. Bellon developed the setup to measure the cantilever's fluctuations in fluids. M. Sepúlveda and F. Aguilar performed experiments and data analysis. L. Bellon developed optimized scripts for data analysis. All authors contributed equally to the paper writing.

Conflicts of Interest

The authors declare no conflict of interest.

References

1. Schilowitz, A. Microcantilever Sensors for Petrochemical Applications. In *Scanning Probe Microscopy for Industrial Applications: Nanomechanical Characterization*; Yablon, D., Ed.; Wiley: Hoboken, NJ, USA, 2014; pp. 251–269.
2. Roberts, I. In-line and on-line rheology measurement. In *Instrumentation and Sensors for the Food Industry*; Kress-Rogers, E., Brimelow, C., Eds.; CRC Press: Cambridge, UK, 2001; pp. 403–422.
3. Harrison, C.; Ryu, S.; Goodwin, A.; Hsu, K.; Donzier, E.; Marty, F.; Mercier, B. A MEMS sensor for the measurement of density-viscosity for oilfield applications. *SPIE Proc.* **2006**, *6111*, 1–11.
4. Cao-Paz, A.; Rodríguez-Pardo, L.; Fariña, J.; Marcos-Acevedo, J. Resolution in QCM Sensors for the Viscosity and Density of Liquids: Application to Lead Acid Batteries. *Sensors* **2012**, *12*, 10604–10620.
5. Boss, C.; Meurville, E.; Sallese, J.; Ryser, P. A viscosity-dependent affinity sensor for continuous monitoring of glucose in biological fluids. *Biosens. Bioelectron.* **2011**, *30*, 223–228.
6. Cakmak, O.; Elbuken, C.; Ermek, E.; Mostafazadeh, A.; Baris, I.; Erdem Alaca, B.; Halil Kavakli, I.; Urey, H. Microcantilever based disposable viscosity sensor for serum and blood plasma measurements. *Methods* **2013**, *63*, 225 – 232.
7. Barnett, C. Measurement and interpretation of synovial fluid viscosities. *Ann. Rheum. Dis.* **1958**, *17*, 234–239.
8. Jalili, N.; Laxminarayana, K. A review of atomic force microscopy imaging systems: Application to molecular metrology and biological sciences. *Mechatronics* **2004**, *14*, 907–945.
9. Dufrene, Y.; Martinez-Martin, D.; Medalsy, I.; Alsteens, D.; Muller, D. Multiparametric imaging of biological systems by force-distance curve-based AFM. *Nat. Methods* **2013**, *10*, 847–854.
10. Butt, H.; Capella, B.; Kappl, M. Force measurements with the atomic force microscope: Technique, interpretation and applications. *Surf. Sci. Rep.* **2005**, *59*, 1–152.
11. Hodges, C. Measuring forces with the AFM: Polymeric surfaces in liquids. *Adv. Colloid Interface Sci.* **2002**, *99*, 13–75.
12. Neuman, R.; Nagy, A. Single-molecule force spectroscopy: Optical tweezers, magnetic tweezers and atomic force microscopy. *Nat. Methods* **2008**, *5*, 491–505.
13. Kadaa, G.; Kienbergera, F.; Hinterdorferb, P. Atomic force microscopy in bionanotechnology. *Nanotoday* **2008**, *3*, 12–19.
14. Lavrik, N.; Sepaniak, M.; Panos, G.D. Cantilever transducers as a platform for chemical and biological sensors. *Rev. Sci. Instrum.* **2004**, *75*, 2229–2253.

15. Tamayo, J.; Kosaka, P.M.; Ruz, J.J.; San Paulo, A.; Calleja, M. Biosensors based on nanomechanical systems. *Chem. Soc. Rev.* **2013**, *42*, 1287–1311.
16. Hutter, J.L.; Bechhoeffer, J. Calibration of atomic-force microscope tips. *Rev. Sci. Instrum.* **1993**, *64*, 1868–1873.
17. Butt, H.; Jaschke, M. Calculation of thermal noise in atomic force microscopy. *Nanotechnology* **1995**, *6*, 1–7.
18. Stark, R.; Drobek, T.; Heckl, W. Thermomechanical noise of a free v-shaped cantilever for atomic-force microscopy. *Ultramicroscopy* **2001**, *86*, 207–215.
19. Paolino, P.; Aguilar Sandoval, F.; Bellon, L. Quadrature phase interferometer for high resolution force spectroscopy. *Rev. Sci. Instrum.* **2013**, *84*, doi:10.1063/1.4819743.
20. Muñoz, R.; Aguilar Sandoval, F.; Wilson C.A.M.; Melo F. Pulling on super paramagnetic beads with micro cantilevers: single molecule mechanical assay application. *Phys. Biol.* **2015**, *12*, doi:10.1088/1478-3975/12/4/046011.
21. Sader, J.E. Frequency response of cantilever beams immersed in viscous fluids with applications to the atomic force microscope. *J. Appl. Phys.* **1998**, *84*, 64–76.
22. Bergaud, C.; Nicu, L. Viscosity measurements based on experimental investigations of composite cantilever beam eigenfrequencies in viscous media. *Rev. Sci. Instrum.* **2000**, *71*, 2487–2491.
23. Papi, M.; Arcovito, G.; de Spirito, M.; Vassalli, M.; Tiribilli, B. Fluid viscosity determination by means of uncalibrated atomic force microscopy cantilevers. *Appl. Phys. Lett.* **2006**, *88*, doi:10.1063/1.2200588.
24. McLoughlin, N.; Lee, S.L.; Hahner, G. Temperature dependence of viscosity and density of viscous liquids determined from thermal noise spectra of uncalibrated atomic force microscope cantilevers. *Lab Chip* **2007**, *7*, 1057–1061.
25. Hennemeyer, M.; Burghardt, S.; Stark, R.W. Cantilever Micro-rheometer for the Characterization of Sugar Solutions. *Sensors* **2008**, *8*, 10–22.
26. Paxman, R.; Stinson, J.; Dejardin, A.; McKendry, R.A.; Hoogenboom, B.W. Using Micromechanical Resonators to Measure Rheological Properties and Alcohol Content of Model Solutions and Commercial Beverages. *Sensors* **2012**, *12*, 6497–6507.
27. Bonfig, K. Das Direkte Digitale Messverfahren als Grundlage einfacher und dennoch genauer und storsicherer Sensoren. *Sensor* **1988**, *3*, 103–108.
28. Matko, V.; Safaric, R. Major Improvements of Quartz Crystal Pulling Sensitivity and Linearity Using Series Reactance. *Sensors* **2009**, *9*, 8263–8270.
29. Matko, V. Next Generation AT-Cut Quartz Crystal Sensing Devices. *Sensors* **2011**, *11*, 4474–4482.
30. Bellon, L. Thermal noise of microcantilevers in viscous fluids. *J. Appl. Phys.* **2008**, *104*, doi:10.1063/1.3021102.
31. Cheng, N. Formula for the Viscosity of a Glycerol Water Mixture. *Ind. Eng. Chem. Res.* **2008**, *47*, 3285–3288.